Ionization delays in few-cycle-pulse multiphoton quantum-beat spectroscopy in helium

Renate Pazourek, Maurizio Reduzzi, Paolo A. Carpeggiani, Giuseppe Sansone, Mette Gaarde, and Kenneth Schafer

Ionization delays in few-cycle pulse multi-photon quantum beat spectroscopy in helium

Renate Pazourek,[1, *] Maurizio Reduzzi,[2, 3] Paolo A Carpeggiani,[2]
Giuseppe Sansone,[2, 3] Mette Gaarde,[1] and Kenneth Schafer[1, †]

[1] *Department of Physics and Astronomy, Louisiana State University, Baton Rouge, Louisiana 70803, USA*
[2] *Dipartimento di Fisica Politecnico Milano, Piazza Leonardo da Vinci 32, 20133 Milano, Italy, EU*
[3] *CNR-IFN Piazza Leonardo da Vinci 32, 20133 Milano, Italy, EU*

We explore quantum beats in the photoelectron signal produced when a bound electron wave packet created by an isolated attosecond pulse is ionized by a delayed, few cycle infrared pulse. Our calculations for helium atoms show that the broad bandwidth of the few cycle pulse creates spectrally overlapping photoelectron peaks that result from one-, two- or three-photon ionization processes. The beat signals can in principle be interferometrically resolved with high resolution, giving access to the relative phase between different multi-photon ionization pathways. For few-cycle NIR fields the relative spectral phases can be extracted over a large energy region and dynamical information becomes available. We find that multi-photon ionization is temporally shifted with respect to one-photon ionization by several hundred attoseconds. Our results also reveal the impact of depletion and resonant pathways on the phase of the quantum beats.

PACS numbers: 32.80.Fb, 32.80.Rm, 42.65.Re, 78.47.jm

I. INTRODUCTION

Attosecond pulses, when interacting with atoms or molecules, create broadband electron wave packets that can be probed, steered and controlled by laser pulses in the visible (VIS) or near-infrared (NIR) regime [1–9]. In order to capture and ultimately control the localized electron motion, it is necessary to be able to reconstruct the excited bound states and their (possibly time-dependent) coherence. Interferometric measurements of electron wavepackets employ one of two methods, which may be present in the same experiment. The first is based on quantum-state holography [10] where a known reference interferes with the unknown wave packet in the detection step but not during the evolution of the electron dynamics of interest. An attosecond holographic setup was proposed in [6] and shown to be able to retrieve the initial wave packet [11]. In that experiment an attosecond pulse was employed to create a wave packet around the ionization threshold in helium and a coherent probe pulse subsequently ionized the bound part which then interfered with the reference continuum wave packet created in the initial excitation step.

The second interferometric method uses quantum-beat spectroscopy where different pathways interfere in the probing step. This is widely used in femtochemistry [12, 13] to study the electronic and vibrational properties of atoms and molecules. A recent example is the characterization of molecular dynamics of small molecules in ultrafast laser fields using Coulomb explosion imaging [14–16]. Quantum beat spectroscopy was used to study the amplitude and phase of dissociating molecular states

as a function of internuclear distance allowing for the visualization of molecular potential energy surfaces. In this paper we study multi-photon ionization to investigate the ionization step itself rather than characterizing the wavepacket before ionization/Coulomb explosion.

We explore a setup similar to that used in [6] for measuring the quantum beats between different bound state contributions but without a reference continuum state, by employing a shaped attosecond pulse that excites states only below threshold. Ionization by a synchronized few-femtosecond NIR probe pulse of medium intensity leads to a plethora of pathways via one-, two- or three-photon ionization that interfere in the continuum. We note that very recently in a similar measurement in helium by Lucchini *et al.* [9] quantum beats between states of mixed parity were reported. In their setup a few-femtosecond XUV pulse consisting of only two harmonics below threshold was used. Here, we use an isolated attosecond XUV pulse and show that careful analysis of the various beating signals reveals that not only the energy difference of the initial states but also that the relative phase can in principle be retrieved with great accuracy. The phase contains rich information not only about the initial wavepacket but also about the ionization process by the NIR itself. For example, for one-photon ionization we find a considerable phase contribution stemming from depletion of the initial wavepacket that occurs for helium singly excited states already for intensities of $1 \cdot 10^{12} \, \text{W/cm}^2$. Similarly, modifications of beating amplitudes due to the intensity of an NIR probing pulse were also seen in neon [17] in an experiment similar to the one proposed here. Simulations based on a few-state model could identify population transfer among bound states and ac Stark shifts by the probing pulse as reasons for the intensity dependence in [17]. Such modifications by the probing step have to be understood for quantum state holography and quantum beat spectroscopy to be a

---

valuable tool. Here we show that establishing a complete understanding of the simple one-photon process also allows us to use it as a reference signal to retrieve phase information about more complicated multi-photon ionization processes.

Retrieving the phase of the ionization step by quantum beat spectroscopy complements other phase measurements in the continuum that have recently been used to gain information on photoemission time delays, like RABBIT ("reconstruction of attosecond beating by interference of two- photon transitions", [2, 18, 19]) and attosecond streaking [1, 20, 21]. Here, however, we operate in a very different regime from those measurements as we are close to threshold with electron kinetic energies ≲ 2 eV. Another fundamental difference is that in attosecond streaking or RABBIT the XUV pulse photoionizes the atom while the IR field serves only as a probe. This probing step contains continuum-continuum transitions which themselves modify the extracted delays. These additional contributions, called Coulomb-laser coupling [22, 23] in the case of streaking and continuum-continuum delay [18, 19] in RABBIT, are very large near threshold, which makes it difficult to model them for low kinetic energies [19, 21]. In the beat spectroscopy setup described here the interference condition is already met after the ionization by the IR field (without absorption of further photons in the continuum). Furthermore, different ionization channels are compared at the same kinetic electron energy for which the phase contribution of the long-ranged part of the potential are identical. Contributions similar to CLC are thus absent.

This paper is organized as follows. In section II we give an overview of our theoretical description, discussing how quantum beat spectrograms can be analyzed and which information becomes available. In section III we focus on the contributions to the spectral phase of the ionized wavepacket within first-order perturbation theory and beyond. Finally in section IV we study which dynamical information can be extracted from quantum beat spectroscopy by investigating interferences involving multi-photon pathways.

Atomic units are used throughout the paper if not stated otherwise.

II. QUANTUM BEAT SPECTROSCOPY

In contrast to previous attosecond holographic experiments [6, 11] we consider the initial state as a pure bound wave packet consisting of a manifold of $1snp$ states (see Fig. 1). Experimentally this can be achieved by filtering the XUV continuum produced by a few-cycle driven HHG source with a Sn filter resulting in a spectrum extending up to 24 eV (the first ionization threshold of helium is 24.56 eV). In the theoretical discussion of this paper we focus on the *non-overlap* region of a delay scan where the NIR pulse arrives long after the XUV pulse. In this case the initial wave packet created by the XUV pulse is well
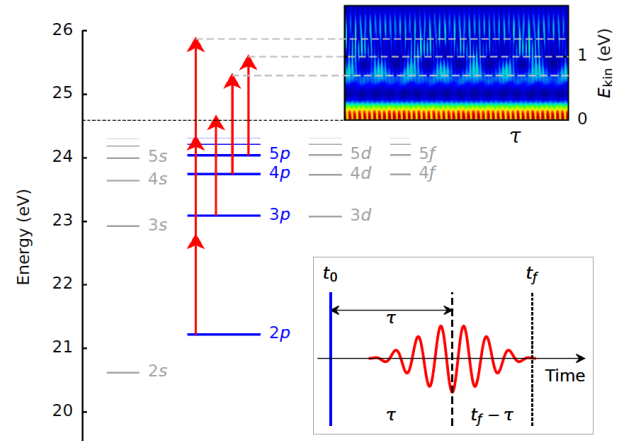

FIG. 1. (Color online) Schematics of multi-photon quantum beat spectroscopy. An attosecond XUV pulse excites at t_0 a bound state wave packet in helium of $1snp$ states subsequently ionized by a delayed NIR probing field (see red arrows and field in the inset). Different quantum paths via absorption of one to three NIR photons interfere in the continuum resulting in a characteristic beating signal.

described by first-order perturbation theory [24],

$$|\psi_i\rangle = -i\sum_n \langle np|\hat{\mathrm{e}}\vec{r}|1s\rangle \tilde{F}_{\mathrm{XUV}}(\tilde{\omega})|np\rangle = \sum_n c_n|np\rangle\,, \quad (1)$$

with the perturbation operator given in length gauge, $\vec{r}\vec{F}_{\mathrm{XUV}}$, and the Fourier transform of the laser field $\tilde{F}_{\mathrm{XUV}}(\tilde{\omega})$ at $\tilde{\omega} = E_{np} - E_0$ (from here on we omit the $1s$ in the notation of singly excited states). In this contribution we assume for simplicity a flat XUV spectrum with a width spanning over the singly-excited states $2p$ to $7p$. Note that states with higher principal quantum number are less populated due to the decreasing excitation cross section. We solve the time-dependent Schrödinger equation (TDSE) for the interaction of the wavepacket with the NIR pulse in the single-active electron approximation (SAE) using a pseudo-spectral split-operator method [25] with a model potential for helium taken from [26]. The energy of the low-lying excited states are adjusted to their experimental values (taken from [27]) during propagation in the spectral basis. In order to obtain the spectral distribution we project the final wave function onto continuum eigenstates of the field-free Hamiltonian. Since we only investigate single excitation/ionization with the second electron remaining in the ground state (~ 20 eV from the first excited state) correlation effects are not expected to be important and the SAE treatment valid. In addition, we note that the doubly excited states in helium are more than 30eV above the first ionization threshold, far away from the energetic region we consider. The linearly polarized laser field has a sine-squared envelope with a FWHM duration of typically 7 fs, a central wavelength of 800 nm and peak intensities between 10^{11} W/cm² and $3\cdot10^{12}$ W/cm².
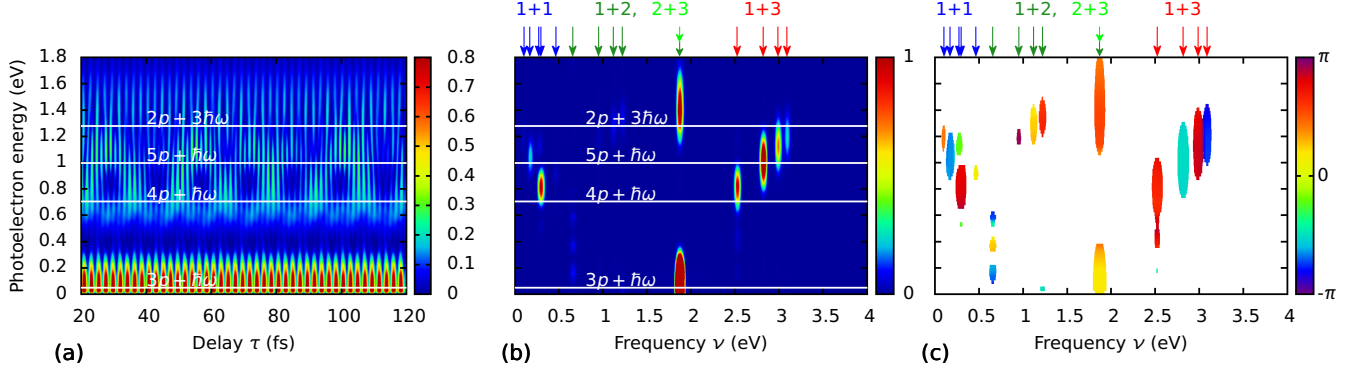
FIG. 2. (Color online) Beating spectrogram (a) and absolute square (b) as well as the argument (c) of the Fourier transform along the delay axis of (a). The initial wave packet was excited at $t_0 = 0$ as a superposition of np states with $n = 2, \ldots, 7$. The 800 nm probing NIR pulse has an intensity of 10^{12} W/cm^2 and duration of 7 fs.

Combining the spectra for different delays τ between the excitation by the XUV and the ionization by the NIR pulse results in a beating spectrogram, Fig. 1 and Fig. 2a. When the width of the short probing pulse (e.g. 0.3 eV for an 800 nm pulse with 7 fs FWHM duration) is larger than the energy spacing of the ionic states two different one-photon pathways can contribute at a given photoelectron kinetic energy, see Fig. 1. This results in interference fringes with a frequency corresponding to the energy difference of the two contributing initial states. The higher lying singly excited $np-$states in helium ($n \geq 3$) are within the bandwidth of the NIR pulse which results in the characteristic beating signal. In other words, the interference condition is met since the probing pulse is short compared to the time scale of the wave packet dynamics to be probed.

This last requirement does not need to be met if we consider interference between pathways with a different number of NIR photons. This is the case for the well separated $2p$ initial state, which can reach similar final energies by absorbing three NIR photons as single-photon ionization of the higher states, leading to the fast beating in Fig. 1 and Fig. 2a. Throughout the paper we will discuss spectra recorded in the *forward* direction along $\theta = 0$. Note that depending on the emission angle, or if the fully-integrated spectra are analyzed, interference between certain pathways may not be observable due to different parity (*cf.* [9]).

For a quantitative analysis of the beatings in the time delay signal (Fig. 2a) we Fourier transform with respect to delay along each final photoelectron kinetic energy. This results in a map of the interference signals as a function of beating frequency ν, and photoelectron energy E, see Fig. 2b. As long as the temporal beating signal can be resolved by the delay step, the spectral analysis reveals the energy differences between the components of the initial wave packet with high resolution. The vertical width of each beating pattern is determined by the spectral overlap of the two contributing pathways, while the horizontal width results from the length of the time series. Beating patterns can be observed for each pair of pathways for which the energy difference of the ionic states is smaller or comparable to the spectral width of the NIR pulse. One-photon ionization of the Rydberg series above $3p$ leads to interference patterns at low energies (see blue arrows in Fig. 2b,c). The beatings at higher frequencies stem from the interference of pathways with a different number of photons, for example $2p$ plus three photons overlaps with one-photon peaks of the higher Rydberg states, red arrows. The beating frequency only depends on the bound state energies, since the ionization by the NIR field is independent of τ in the non-overlap region that we consider.

The origin of the beating signal as well as the information contained therein can be understood by looking at an initial wave packet that for simplicity only consists of two bound states α and β. The wave packet at the arrival time τ of the NIR pulse reads

$$|\psi_f(\tau)\rangle = c_\alpha e^{-iE_\alpha \tau}|\alpha\rangle + c_\beta e^{-iE_\beta \tau}|\beta\rangle, \qquad (2)$$

where c_n, $n = \alpha, \beta$, are the initial amplitudes after absorption of the XUV photon at time $t_0 = 0$. The transition amplitude after ionization by the NIR pulse to the continuum energy E at time t_f is given by

$$a_E(t_f) = \left[c_\alpha e^{-iE_\alpha \tau} C_{\alpha,E} + c_\beta e^{-iE_\beta \tau} C_{\beta,E} \right] e^{-iE(t_f - \tau)}, \qquad (3)$$

where $C_{n,E}$ describes the ionization step by the NIR. The spectrum reads

$$P(E,\tau) = |a_E(t_f)|^2 = |M_\alpha(E)|^2 + |M_\beta(E)|^2$$

$$+ |M_\alpha(E)| |M_\beta(E)| \cos\left[(E_\alpha - E_\beta)\tau + \Delta\varphi(E) \right], \quad (4)$$

where we combined the two amplitudes, $M_n(E) = c_n C_{n,E}$. In Fig. 3 we show $|M_n(E)|^2$ and $\arg M_n(E)$ for

different initial states and ionization pathways. Note that the arg $M_n(E)$ are not directly available in experiments. However, as long as both M_n in Eq. 4 do not vanish at a given final energy E we see an interference signal at frequency $\Delta E = E_\alpha - E_\beta$ (see Fig. 2) with a possible phase offset

$$\Delta\varphi(E) = \Delta\phi_i + \Delta\phi_f(E) \tag{5}$$

which becomes accessible in the experimental setup, see Fig. 2c. Here $\Delta\phi_i$ is the phase difference of the components of the initial wave packet (Eq. 1) while $\Delta\phi_f$ is the phase difference accumulated in the ionization step. If no additional phases are accumulated in the ionization process ($\Delta\phi_f(E) = 0$) it was shown in [11] that the phases of the initial wave packet can be retrieved. Here we go a step further and ask the question what additional information is encoded in the beating phases, especially for the more complicated multi-photon ionization by the NIR pulse.
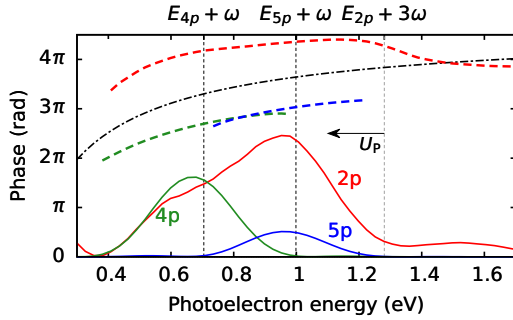

FIG. 3. (Color online) Spectral phase and spectrum after ionization of a pure $4p$ or $5p$ initial state by one NIR photon and $2p$ with three NIR photons. The laser pulse has a duration of $7\,\text{fs}$ and intensity $3 \cdot 10^{12}\,\text{W/cm}^2$. The black dashed-dotted line shows the perturbative limit Eq. 8.

In Fig. 2c we show the argument of the Fourier transform wherever there is a significant signal (see the absolute square value in Fig. 2b). Since the horizontal extension of the Fourier beatings only stems from the finite time series the only valuable information is in the phase variation along the photoelectron energy axis. This vertical extension represents the energy region over which we can retrieve the (difference) phase of two quantum pathways. In the following, we exploit the fact that the phase is available over a large energy region to gain information about the dynamics of the ionization process that would not be available in a single point. Moreover, the Fourier analysis reveals a plethora of different beating signals that can be grouped together depending on the number of NIR photons involved. States in the initial wave packet that lie within the bandwidth of the ionizing pulse interfere in lowest order with the absorption of one NIR photon each. These can be found at low frequencies ($\nu \lesssim \Delta\omega$) and are labelled "1+1" in Fig. 2b,c. Since we

analyze the spectrogram along a certain direction (parallel to the laser polarization) interferences from pathways with mixed parity, "1+2" and "2+3" are also visible (note that they would be absent in an angle-integrated spectrogram). The binding energy of the $2p$ state is about $3\,\text{eV}$ lower than the higher states so that it overlaps with the Rydberg series by the absorption of two more photons leading to the high frequency beatings, labeled "1+3". In order to observe those high-frequency beatings in experiments the carrier-envelope phase (CEP) must be stabilized. For a short pulse, variation of the CEP has a similar effect as a temporal shift of the pulse envelope, i.e., in our setup a change in the delay τ between the two pulses. Averaging over different CEPs thus washes out all oscillations faster than the NIR field so that beatings with frequencies $> \hbar\omega$ can not be observed without CEP stabilization.

A lineout for two different beating frequencies in Fig. 2c is shown in Fig. 4. Since in our setup $\Delta\phi_i = 0$, this amounts to the difference $\Delta\phi_f(E)$ of the phases accumulated in the ionization process. We observe a quite different behaviour for the "1+1" beating ($4p - 5p$) and the "1+3" ($2p - 5p$) as well as a large intensity dependence, showing that the ionization step indeed can not be ignored, but on the contrary is of interest on its own.
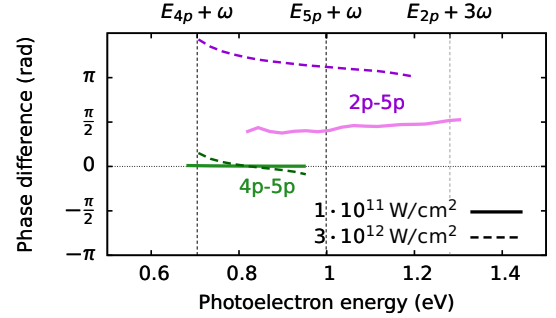

FIG. 4. (Color online) Extracted beating phase $\Delta\varphi(E)$ with $\Delta\phi_i = 0$ (Eq. 4, Eq. 5) for the beating between $4p + \gamma$ and $5p + \gamma$ and the higher order process $2p + 3\gamma$ and $5p + \gamma$ for a laser intensity of $I = 3 \cdot 10^{12}\,\text{W/cm}^2$. Note that in the original data in Fig. 2c the phases are shifted by a constant phase depending on the actual time t_0.

III. SPECTRAL PHASE FOR ONE-PHOTON IONIZATION BY A STRONG NIR FIELD

The spectral phases of photoelectrons contain information about the atomic system as well as the dynamics of the ionization process. In the following, we analyze the spectral phase of the final state within lowest-order perturbation theory. The first-order perturbation theory

amplitude for one-photon ionization reads

$$a_{i \to f}^{(1)} = -i \int_{t_0}^{t_f} \mathrm{d}t' e^{iE_f(t'-t_f)} \langle f|\hat{V}(t')|i\rangle e^{-iE_i(t'-t_0)} . \quad (6)$$

The interaction with the laser field (the perturbation) is given by $\hat{V}(t) = \hat{e}\vec{r}F(t)$. We assume for now that the time t_0 when the initial wave packet $|i\rangle$ was excited by the XUV pulse is known and set it to $t_0 = 0$. In general, the absolute delay is not known in experiment, however, we will discuss later how in our scheme this problem can be circumvented. For a time t_f after the end of the pulse, the time integral in Eq. 6 can be formally taken from $-\infty$ to ∞ (when $F(t < t_0) = F(t > t_f) = 0$) and as such it is the Fourier transform of the laser field. The amplitude (Eq. 6) then follows as

$$a_{i \to f}^{(1)} = -i\langle f|\hat{e}\vec{r}|i\rangle e^{-iE_i\tau} e^{-E_f(t_f-\tau)} \tilde{F}(\omega) , \quad (7)$$

where we have assumed that the laser field is symmetrically centered around τ and explicitly write out all phases so that the Fourier transform of the field, $\tilde{F}(\omega > 0)$, is real and $\omega = E_f - E_i$. Comparing Eq. 7 with Eq. 3 reveals that $C_{n,E} = -i\langle f|\hat{e}\vec{r}|n\rangle \tilde{F}(\omega)$. The accumulated phase $\varphi_n^{(1)} = \arg a_{i \to f}^{(1)}$ for a pure initial state $|i\rangle = |n\rangle$,

$$\varphi_n^{(1)} = -\frac{\pi}{2} + \arg \langle f|\hat{e}\vec{r}|n\rangle - E_i\tau - E_f(t_f - \tau) \quad (8)$$

then consists of the scattering phase shift contained in the dipole transition matrix element and the free propagation phases before and after the pulse (see inset of Fig. 1).
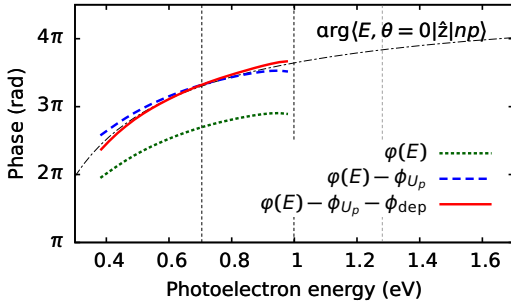

FIG. 5. (Color online) Argument $\varphi(E)$ of the final wave function for the solution of the TDSE for ionization of an initial $4p$ state compared to the argument of the corresponding transition matrix element and non-perturbative corrections (see text) for a laser intensity of $I = 3 \cdot 10^{12}\,\mathrm{W/cm}^2$.

The resulting beating phase $\Delta\varphi(E)$ in Eq. 5 for an initial wave packet $|i\rangle = \sum_n c_n|np\rangle$ follows as

$$\Delta\phi_i = \arg c_\alpha - \arg c_\beta \quad (9a)$$

$$\Delta\phi_f(E) = \arg \langle f|\hat{e}\vec{r}|\alpha\rangle - \arg \langle f|\hat{e}\vec{r}|\beta\rangle . \quad (9b)$$

In the following discussion we assume a flat phase for the initial wave packet ($c_n(t_0) \in \mathbb{R}$ in Eq. 1) and hence $\Delta\phi_i = 0$ and $\Delta\varphi = \Delta\phi_f$. The final state $|f\rangle$ is a single continuum state $|E\ell\rangle$, or $|E\theta\rangle$ for the spectra along one direction θ, respectively. Since $\arg\langle E\ell|\hat{e}\vec{r}|np\rangle$ only depends on the scattering phase of the final state it is independent of the principle quantum number n. Following Eq. 9 we expect $\Delta\varphi(E)$ to approximately vanish in the perturbative regime. For the beating between $4p$ and $5p$ shown in Fig. 4, $\Delta\varphi(E)$ indeed nearly vanishes for lower intensities while we observe modifications for higher intensities, especially at the ends of the overlap region. In the nonperturbative regime we find that the phases of the final wave function of the individual p-states in Fig. 3 deviate from the perturbative limit (Eq. 8) for intensities $\gtrsim 1 \cdot 10^{12}\,\mathrm{W/cm}^2$. We have also checked that for $I \lesssim 1 \cdot 10^{11}\,\mathrm{W/cm}^2$ the solution of the TDSE agrees perfectly with the perturbative limit.

We can identify two main effects that become important for higher intensities: (i) the ponderomotive shift is not negligible anymore and (ii) the initial wave packet gets depleted. Both manifest themselves in the phase of the final wave packet. The ponderomotive shift for a free electron is given by $U_\mathrm{P} = I/4\omega^2$ which amounts to $0.18\,\mathrm{eV}$ for $800\,\mathrm{nm}$ and $I = 3 \cdot 10^{12}\,\mathrm{W/cm}^2$. We therefore expect a shift of the spectrum to lower energies. In Fig. 3 we see that the spectrum of an initial $2p$ state is indeed shifted from the expected position at $E_{2p} + 3\omega$. The shift is even larger than U_P due to the nearly resonant transition over np and nf states in the three-photon process. The one-photon spectrum of the $4p$ and $5p$ initial states, though, is only marginally shifted. For the higher Rydberg states we have to take into account their AC-Stark shift. In the limit of highly excited states, where the energy difference of neighboring states becomes small compared to the frequency of the IR field and the field strengths are subatomic, the AC-stark shift becomes identical to U_P [28]. From this it follows that the shift of the initial and final state cancel in the photoelectron spectrum (note that the slight shift to lower energies is due to the cross section which strongly decreases as a function of energy).

In contrast, the effect of the ponderomotive shift of the initial and final state energies, $E_{np} \to E_{np} - U_\mathrm{P}$ and $E_f \to E_f - U_\mathrm{P}$, adds up in the propagation phase Eq. 8. For a Rydberg state this additional phase can be approximated by the ponderomotive shift over the effective duration of the laser pulse, T_eff,

$$\phi_{U_\mathrm{P}} = U_\mathrm{P}T_\mathrm{eff} , \quad T_\mathrm{eff} = \int_{-\infty}^{\infty} F^2(t)\mathrm{d}t/I_0 \quad (10)$$

where I_0 is the peak intensity of the laser field. For an intensity of $3 \cdot 10^{12}\,\mathrm{W/cm}^2$ this is already a considerable, yet constant, phase shift for each individual state, see Fig. 5. It is the same for all the easily polarizable Rydberg states and hence cancels in the relative final phase $\Delta\phi_f$, and thus in the total phase difference $\Delta\varphi$ observed in the beating spectrogram (Fig. 4) for '1+1' photon pro-

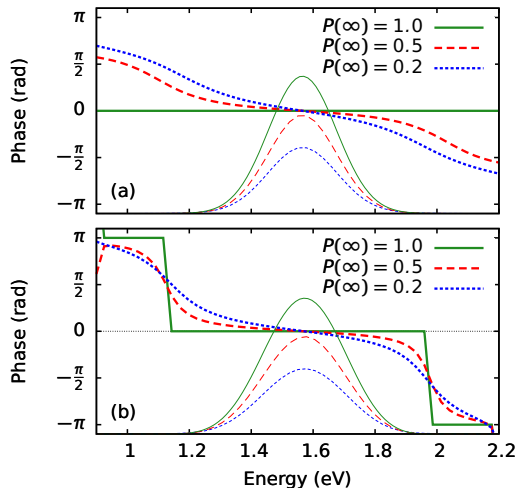cesses but not for '1+3' photon processes.

FIG. 6. (Color online) Additional phase (thick lines) due to depletion of the initial state: (a) $\pm\pi/2$ shift over the bandwidth for pulses with a Gaussian envelope and (b) $\pm\pi$ shift at the zeros of the spectrum for a sine-squared envelope function. The corresponding pulse spectra are shown with the thin lines (arbitrary scale).

Depletion of the initial state further modifies the ionization process beyond the perturbative limit. For the example shown in Fig. 5 for ionization of an initial $4p$ state by an NIR field of $3 \cdot 10^{12}$ W/cm^2 only 27% of the initial population is left after the end of the pulse and so depletion can not be ignored. On an intuitive level we would expect more ionization at the beginning of the pulse than at the end and hence an effective shift of the ionization time. Formally, a phase is introduced since already an infinitesimal amount of depletion breaks the time-symmetry of the ionization process and hence the Fourier transform in Eq. 7 can not be real anymore. In a lowest-order treatment, we include the depletion into the first-order perturbation theory amplitude by assuming that the initial state is decaying. We replace $|i\rangle$ in Eq. 6 with a time-dependent initial state $\sqrt{P_i(t)}|i\rangle$ where the time-dependent probability $P_i(t)$ is given by

$$P_i(t) = \exp\left[-a \int_{-\infty}^{t} F^2(t')\mathrm{d}t'\right] \qquad (11)$$

with a being proportional to the cross section per unit energy. The integral can be solved analytically and yields for a Gaussian pulse envelope with a FWHM duration of T

$$P_i(t) = \exp\left[\frac{\log P_i(\infty)}{2}\left(1 + \mathrm{erf}\left[t\sqrt{\log 16}/T\right]\right)\right]. \quad (12)$$

Including the decay rate into Eq. 6 results in a modified Fourier transform of the laser field shown in Fig. 6. While the amplitude only gets diminished by an overall

scaling factor, the phase shows a dramatic change. Near the center frequency the phase has a nearly linear slope corresponding to a time shift of the ionization since more ionization takes place in the first part of the pulse. The less intuitive part is the phase transition of π that occurs for a Gaussian pulse over the spectral width, Fig. 6a. Already for an infinitesimal amount of depletion the integrand in Eq. 6 becomes asymmetric which together with the Gaussian pulse enforces this π phase change. Due to the finite temporal length, the Fourier transform of a sine-squared envelope function always contains zeros in the spectrum, which causes π phase jumps at every zero crossing (see phase for $P(\infty) = 1.0$ in Fig. 6b). Including the depletion then smears out these jumps.

The phase modifications are minimal at the center of the spectral width which is probably the reason why they have never been observed, to the best of our knowledge. In our proposal, however, since we observe the phase difference in the overlap region we need the phase over a wider range and hence we observe distortions at off-center frequencies. Combining the effects of the ponderomotive shift, ϕ_{U_P}, and depletion, ϕ_{dep}, indeed mostly explains the difference between the atomic phase from the dipole transition and the solution of the TDSE for the $4p$ initial state shown in Fig. 5. We note, however, that for increasing n the agreement of the actual phase with our model including ponderomotive shift and depletion gets worse. Since those higher lying states are highly polarizable and have strong couplings to other bound states while the ionization cross section decreases, we suspect further phase distortions that go beyond the simple modeling presented here.

One possibility of minimizing the laser-induced phase distortions is the use of lower NIR intensities. For example, for $I = 1 \cdot 10^{12}$ W/cm^2 64% of the population is left in an initial $4p$ state as compared to 27% for $I = 3 \cdot 10^{12}$ W/cm^2. However, since we are interested in multi-photon beatings lower intensities diminish the three photon signals. The other possibility is the use of shorter NIR pulses with a larger spectral width. This helps in two ways, first the depletion is reduced and second the different pathways overlap in a much broader region so that the center of the overlap is not at the edge of the spectral width.

IV. MULTI-PHOTON QUANTUM BEATS

As we have seen, the relative beating phases for one-photon processes contain information about the strong-field modifications of the ionization process. We can now pose the question to what extent dynamical information for multi-photon processes becomes accessible. In Fig. 7, we show the extracted phase difference for the higher order processes $2p + 3\gamma$ and $3p + 2\gamma$ both beating against the various overlapping one-photon ionized Rydberg states for a laser intensity of 10^{12} W/cm^2. Since the
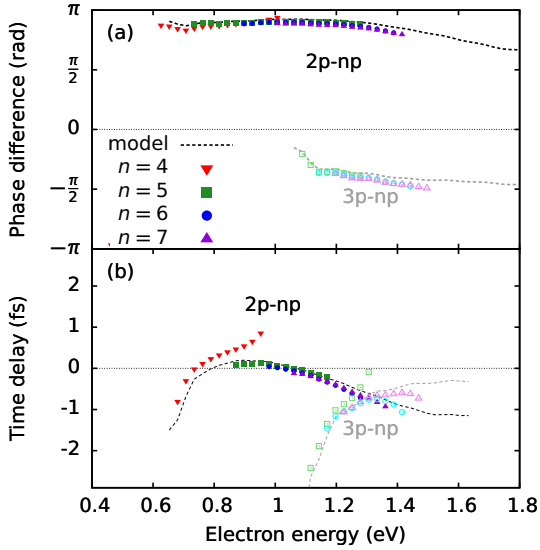
FIG. 7. (Color online) (a) $\Delta\varphi(E)$ for the higher order processes $2p + 3\gamma$ (full symbols) and $3p + 2\gamma$ (open symbols) both beating against Rydberg states with $n = 4, 5, 6, 7$. The model (black dashed line) is based on the difference of the spectral phase for the $2p$ or $3p$ ionization alone and the argument of the one-photon dipole matrix element. The relative phases are corrected by the actual time zero, $\Delta E \cdot t_0$, for $\tau \to \tau - t_0$ in Eq. 4. (b) Relative time delay, $\partial \Delta\varphi(E)/\partial E$, between one- and multi-photon ionization including the model (black dashed lines) as in (a). The laser had a duration of 7 fs and an intensity of 10^{12} W/cm^2.

distortion of the one photon phases are minimal at this intensity we find perfect agreement between the different Rydberg states for $n = 4, 5, 6, 7$. We recall that the one photon signal in the perturbative regime coincides with the argument of the dipole transition element (see Eq. 8). The extracted phase difference hence shows all phase contributions in addition to the atomic scattering phase. Directly subtracting the scattering phase from the numerically extracted spectral phase for an initial $2p$ state ("model" in Fig. 7) is in near perfect agreement with the phase difference extracted from the beating signal. The spectral phase also allows us to extract dynamical information about the ionization process. In general the time (group) delay of a wavepacket is given by the spectral derivative of its complex argument or phase. In the case of scattering, the time delay has been first described by Eisenbud, Wigner and Smith [29–31] and has evolved as the key physical observable describing time-resolved photoemission (see e.g. [21] and references therein).

The additional delay due to multi-photon ionization is shown in Fig. 7b. We note that numerical convergence for the spectral phase is very slow for the multi-photon wavepacket. In particular, we observe unphysical oscillations in the phase which are enhanced in the time delay and depend on the radial extension of the numerical box. Since those oscillations are exactly out of phase for oppo-

site directions of the photoelectron, we show the forward-backward averaged time shifts which no longer show a variation with the grid size used. The additional multi-photon ionization delay, $\partial\Delta\phi_f(E)/\partial E$, i.e., the emission time difference between the two beating states is found to be varying between -2 fs and slightly positive delays for the $2p - np$ and $3p - np$ signal in Fig. 7b. Looking at the energy level diagram in Fig. 1 reveals that absorbing two photons from the $2p$ state is resonant with the higher lying states close to threshold. From there absorption of the third photon leads to ionization. For such a sequential process one would expect that an arbitrary amount of time can pass between the absorption of the photons. On average, this leads to an effectively delayed ionization, *i.e.*, it takes longer to absorb three than just one photon from the NIR pulse. This is indeed the case for NIR wavelengths longer than those we have concentrated on in this paper. For such wavelengths, we find that the three-photon ionization process is effectively delayed relative to the one-photon ionization process by > 1 fs for 900 nm. However, unlike the expected sequential behaviour we find for our results with an NIR intensity of $1 \cdot 10^{12}$ W/cm^2 (Fig. 7b) "advanced" (negative time shifts) rather than "delayed" emission for the $2p-np$ beating signal. Even more negative time shifts can be found for the beating between $3p$ plus two NIR photons with the one-photon signals of higher np-states. $3p$ plus one NIR photon excites the system around the ionization threshold so that sequential pathways should be open as well. We suspect that in this case depletion of the initial state (for $1 \cdot 10^{12}$ W/cm^2 only 35% is left in the $3p$ state) plays a dominant role. A further indication is the change of the beating phase for higher intensities shown in Fig. 8. For both the $2p+3\gamma$ and the $3p+2\gamma$ processes the time shift is getting more negative for higher intensities, which as we have seen, is the typical behaviour for an additional depletion phase. As mentioned earlier, the effect of depletion can be reduced by using a shorter NIR pulse with the additional advantage of a wider available energy range. Indeed for a pulse with a FWHM duration of only 4 fs the intensity variation is greatly reduced, see Fig. 8c,d. Moreover, we find that the emission for the $2p$ process is indeed delayed as expected for the sequential process up to intensities of $2 \cdot 10^{12}$ W/cm^2.

Varying not only the intensity and duration, but also the wavelength of the NIR pulse reveals a strong wavelength and energy dependence of the time shifts and delayed emission for longer wavelengths of about 900 nm. We believe that this is due to a strong sensitivity to the available resonant transitions. Extraction of the transient population in the Rydberg states during the propagation indeed revealed a strong two-photon coupling between the $2p$ and higher excited states and we see the onset of Rabi-flopping. Depending on the intensity and duration of the laser pulse, large amounts of population can therefore get transferred to higher lying f-states, for which the ionization cross section is very small (see for example [32, 33]). For the parameters used here this strong
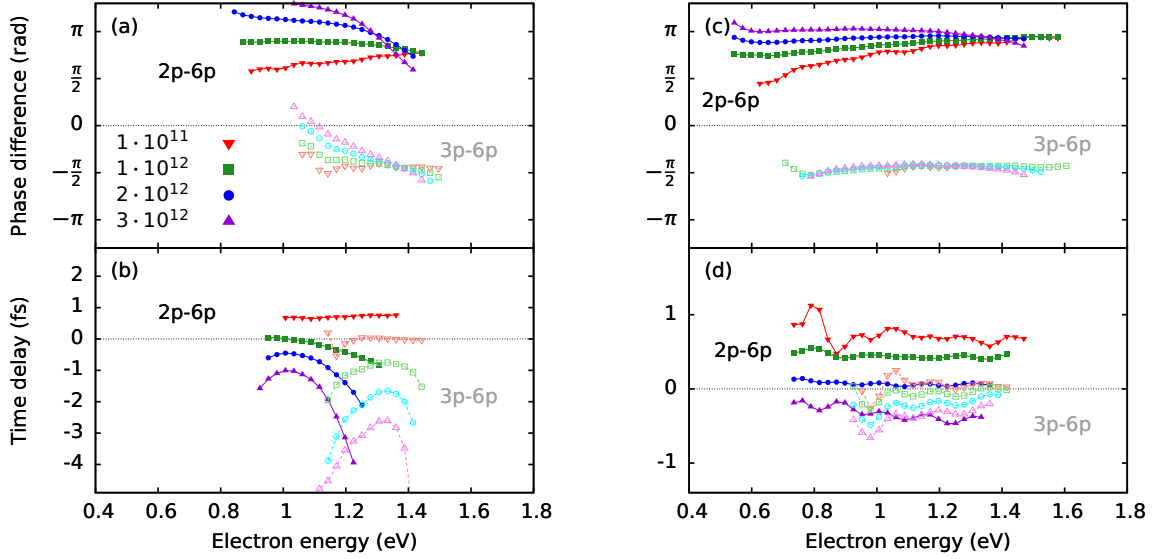
FIG. 8. (Color online) $\Delta\varphi(E)$ for the higher order processes $2p+3\gamma$ and $3p+2\gamma$ both beating against $6p$ for (a) 7 fs and (c) 4 fs duration of the NIR pulse. The relative phases are corrected by $\Delta E \cdot t_0$. (b) and (d) show the corresponding relative time delays. The shift to more negative time delays for higher intensities reflects the fact that the initial state gets depleted by the NIR pulse. The symbols and colors for the different intensities are found in (a) for all panels. Full symbols are used for the beating with the $2p$ state and open symbols for the $3p$ state. The NIR intensity is $10^{12}\,\mathrm{W/cm^2}$.

coupling nearly empties the initial $2p$ state into long-lived high-lying $f-$states. Ionization via (non)resonant channels not involving such long-lived states is thus more probable in the beginning of the pulse as long as the $2p$ state is still populated. We believe that this is the reason for the unexpected advanced emission for the 800 nm pulse of 7 fs investigated here. Even though it is tempting to interpret all the phase modifications as temporal shifts of the ionization process, higher order phases corresponding to a chirp or even more complicated behaviour often lack such simple explanations. Further discussion into this direction, however, goes beyond the scope of this work.
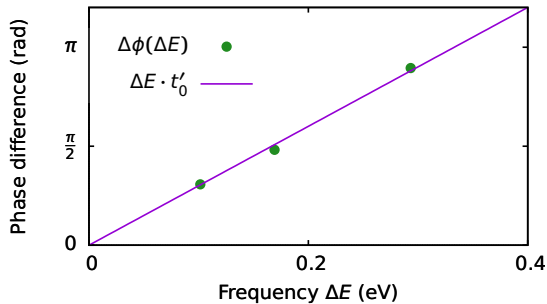

FIG. 9. (Color online) Extraction of t_0 for three '1+1' photon beatings and a 7 fs pulse with $I = 10^{12}\,\mathrm{W/cm^2}$. We assumed a phase offset of $t_0 = 6000$ as. The linear fit $\Delta\varphi(\Delta E) = \Delta E t_0'$ results in $t_0' = 6207$ as.

Finally, we discuss the experimental feasibility of the proposed setup. While the delay step can usually be controlled on the ten attoseconds level the absolute delay between XUV and NIR pulse is very difficult to obtain. Since the beating in Eq. 4 is given by $\Delta E \cdot (\tau - t_0)$ the actual time t_0 adds a phase of $\Delta E \cdot t_0$ to our final phase difference $\Delta\varphi(E)$. In our scheme this poses a problem, since all the beating frequencies ΔE are different. Note that this is not the case for other interferometric pump-probe setups like e.g. RABBIT which uses an attosecond pulse train. In that case dynamical information is extracted from the beating phase of the various sidebands which are all modulated by 2ω so that the additional phase $2\omega t_0$ is the same for each sideband. In our scheme we can exploit the fact that the beating phase between one-photon processes should be zero so we can use them as a reference to extract the actual time t_0 of the experiment. In principle already one point would suffice to extract t_0 from the condition $\Delta\varphi(\Delta E) = \Delta E \cdot t_0$ in the absence of the 2π ambiguity. Using at least two different beating frequencies allows us to extract t_0 from the derivative $\partial\Delta\varphi(\Delta E)/\partial\Delta E$ as long as the phase does not change by more than 2π. This condition can be met if t_0 is approximately known. For the beating frequencies of the one photons signals that are below $0.3\,\mathrm{eV}$ there is no ambiguity for $t_0 < 13\,\mathrm{fs}$ which is longer than the NIR pulses used. In Fig. 9 we demonstrate this for the example of the three lowest '1+1' beatings where we assumed an offset of t_0 by 6000 as. The linear fit retrieves a value of $t_0' = 6207$ as which amounts to a phase error of 0.15π.

V. CONCLUSIONS

In summary, we have shown that the proposed attosecond quantum beat spectroscopy setup is capable of extracting the spectral components of an initial wave packet as well as the relative phases of different ionization processes. The observed spectral phases of the ionized wave packets can be well described within first-order perturbation theory for one-photon transitions and intensities below $10^{12}\,\mathrm{W/cm^2}$. For higher intensities we showed that the ponderomotive shift and depletion of the initial wavepacket modify the phase. This allowed us to draw conclusions about the dynamics of the ionization process. Especially for the investigated multi-photon ionization processes we observed large time shifts that stem from sequential ionization via intermediate bound states.

[1] M. Hentschel, R. Kienberger, C. Spielmann, G. A. Reider, N. Milosevic, T. Brabec, P. Corkum, U. Heinzmann, M. Drescher, and F. Krausz, Nature **414**, 509 (2001).

[2] P. M. Paul, E. S. Toma, P. Breger, G. Mullot, F. Auge, P. Balcou, H. G. Muller, and P. Agostini, Science **292**, 1689 (2001).

[3] P. B. Corkum and F. Krausz, Nat. Phys. **3**, 381 (2007).

[4] T. C. Weinacht, J. Ahn, and P. H. Bucksbaum, Nature **397**, 233 (1999).

[5] P. Johnsson, J. Mauritsson, T. Remetter, A. L'Huillier, and K. J. Schafer, Phys. Rev. Lett. **99**, 233001 (2007).

[6] J. Mauritsson, T. Remetter, M. Swoboda, K. Klünder, A. L'Huillier, K. J. Schafer, O. Ghafur, F. Kelkensberg, W. Siu, P. Johnsson, M. J. J. Vrakking, I. Znakovskaya, T. Uphues, S. Zherebtsov, M. F. Kling, F. Lépine, E. Benedetti, F. Ferrari, G. Sansone, and M. Nisoli, Phys. Rev. Lett. **105**, 053001 (2010).

[7] N. Shivaram, H. Timmers, X. M. Tong, and A. Sandhu, Phys. Rev. Lett. **108**, 193002 (2012).

[8] S. Chen, M. Wu, M. B. Gaarde, and K. J. Schafer, Phys. Rev. A **87**, 033408 (2013).

[9] M. Lucchini, A. Ludwig, T. Zimmermann, L. Kasmi, J. Herrmann, A. Scrinzi, A. S. Landsman, L. Gallmann, and U. Keller, Phys. Rev. A **91**, 063406 (2015).

[10] C. Leichtle, W. P. Schleich, I. S. Averbukh, and M. Shapiro, Phys. Rev. Lett. **80**, 1418 (1998).

[11] K. Klünder, P. Johnsson, M. Swoboda, A. L'Huillier, G. Sansone, M. Nisoli, M. J. J. Vrakking, K. J. Schafer, and J. Mauritsson, Phys. Rev. A **88**, 033404 (2013).

[12] A. H. Zewail, *Femtochemistry: Ultrafast Dynamics of the Chemical Bond (World scientific Series in 20th Century Chemistry)*, Vol. 3 (World Scientific, 1994).

[13] A. H. Zewail, J. Phys. Chem. A **104**, 5660 (2000).

[14] B. Feuerstein, T. Ergler, A. Rudenko, K. Zrost, C. D. Schröter, R. Moshammer, J. Ullrich, T. Niederhausen, and U. Thumm, Phys. Rev. Lett. **99**, 153002 (2007).

[15] M. Winter, R. Schmidt, and U. Thumm, New J. Phys. **12**, 023020 (2010).

[16] S. De, M. Magrakvelidze, I. A. Bocharova, D. Ray, W. Cao, I. Znakovskaya, H. Li, Z. Wang, G. Laurent, U. Thumm, M. F. Kling, I. V. Litvinyuk, I. Ben-Itzhak, and C. L. Cocke, Phys. Rev. A **84**, 043410 (2011).

[17] H. Geiseler, H. Rottke, G. Steinmeyer, and W. Sandner, Phys. Rev. A **84**, 033424 (2011).

[18] K. Klünder, J. M. Dahlström, M. Gisselbrecht, T. Fordell, M. Swoboda, D. Guénot, P. Johnsson, J. Caillat, J. Mauritsson, A. Maquet, R. Taïeb, and A. L'Huillier, Phys. Rev. Lett. **106**, 143002 (2011).

[19] J. M. Dahlström, A. L'Huillier, and A. Maquet, J. Phys. B **45**, 183001 (2012).

[20] M. Schultze, M. Fiess, N. Karpowicz, J. Gagnon, M. Korbman, M. Hofstetter, S. Neppl, A. L. Cavalieri, Y. Komninos, T. Mercouris, C. A. Nicolaides, R. Pazourek, S. Nagele, J. Feist, J. Burgdörfer, A. M. Azzeer, R. Ernstorfer, R. Kienberger, U. Kleineberg, E. Goulielmakis, F. Krausz, and V. S. Yakovlev, Science **328**, 1658 (2010).

[21] R. Pazourek, S. Nagele, and J. Burgdörfer, Rev. Mod. Phys **87**, 765 (2015).

[22] C. H. Zhang and U. Thumm, Phys. Rev. A **82**, 043405 (2010).

[23] S. Nagele, R. Pazourek, J. Feist, K. Doblhoff-Dier, C. Lemell, K. Tőkési, and J. Burgdörfer, J. Phys. B **44**, 081001 (2011).

[24] B. H. Bransden and C. J. Joachain, *Physics of atoms and molecules* (Longman New York, 1983).

[25] X. M. Tong and S. I. Chu, Chemical Physics **217**, 119 (1997).

[26] X. M. Tong and C. D. Lin, J. Phys. B **38**, 2593 (2005).

[27] W. C. Martin, Phys. Rev. A **36**, 3575 (1987).

[28] N. B. Delone and V. P. Krainov, Physics-Uspekhi **42**, 669 (1999).

[29] L. Eisenbud, *Formal properties of nuclear collisions*, Ph.D. thesis, Princeton University (1948).

[30] E. P. Wigner, Phys. Rev. **98**, 145 (1955).

[31] F. T. Smith, Phys. Rev. **118**, 349 (1960).

[32] M. P. de Boer and H. G. Muller, Phys. Rev. Lett. **68**, 2747 (1992).

[33] K. J. Schafer and K. C. Kulander, Laser Physics **7**, 740 (1997).